Spectrally Pure W-Band RF Carrier Generation with Packaged Silicon Photonics Circuit

Claudio Porzi, Marco Chiesa, Alessandra Bigongiari, Aina Serrano Rodrigo, Marc Sorel, Davide Rotta, Luca Roselli, Antonio D'Errico, Antonella Bogoni, and Antonio Malacarne

***Abstract*—A packaged silicon photonics radio-frequency (RF) synthesizer operating in the millimeter (mm-) wave band suitable for clock signal distribution in b5G/6G radio access networks is realized and experimentally characterized. The assembly include a photonic integrated circuit (PIC) acting as a frequency multiplier for a local oscillator (LO) reference at microwave frequencies and a printed circuit board (PCB) hosting a custom bias tee designed to provide a wideband matching condition over more than 6 GHz around 20 GHz for the input LO signal and supporting high power levels for efficient frequency multiplication operation. Measurements performed on a 100 GHz generated RF signal via five-fold multiplication of a LO wave at 20 GHz indicate a low phase noise level of -97 dBc/Hz at an offset of 10 kHz from the carrier with a limited excess timing jitter of less than 2 fs with respect to the LO signal, making the circuit operating nearly as an ideal frequency multiplier.**

***Index Terms*—Millimeter-wave band, sub-THz band, integrated microwave photonics, silicon photonics, photonic integrated filters.**

I. Introduction

In THE recent past years, photonic-integrated radio-frequency (RF) synthesizers operating in the millimeter (mm-)wave band and above have received considerably increasing interest [1], [2], [3], [4], [5], [6], [7]. Using microwave photonics techniques for generating electrical carriers through the beating in a fast photodiode (PD) of two optical carriers brings indeed into the system advantages like wideband reconfigurability, low phase noise (PN), and the possibility of low loss fiber distribution [8], [9], [10]. By combining these unique features with the reduction of fabrication costs and power consumption associated with system miniaturization, photonic integrated circuit (PIC) technologies can thus effectively support the deployment of several emerging applications in the fields of modern communications, imaging, and sensing systems [11].

We recently demonstrated programmable high-quality RF synthesis from the Ku- up to the W-band (i.e., a tuning range from about 40 to 110 GHz, limited by the available equipment) in a PIC realized with monolithic silicon on insulator technology through CMOS-compatible fabrication process [6]. With respect to other recent photonic integrated solutions operating in the mm-wave/sub-THz bands, the proposed implementation permits to reach low levels of PN that would not be possible using free-running on-chip lasers in hybrid technology [1], [4], or relatively large-linewidth monolithic dual-wavelength sources [2], [3], [7]. Instead, we adopt a scheme in which a beating tone that is inherently coherent with an original laser carrier is selected out from an optical frequency comb (OFC) whose RF noise features are related to a reference microwave local oscillator (LO) [12]. By on-chip integration of tunable filters and OFC source, this approach can be made flexible and compact [5], [6]. However, practical systems applications also require advanced packaging solutions for the photonic core chip ensuring LO signal integrity, efficient thermal dissipation, low optical insertion loss, along with improved robustness and stability.

In [13], we have shown the preliminary characterization of a second-generation version of the photonic circuit presented in [6], [14], exhibiting optimized performance and specifically designed for being fully packaged. The related design of a printed circuit board (PCB) encompassing a matching network for efficient delivery of the LO signal driving the PIC and of all the required DC control signals has also been introduced. Here, the details of the developed circuit are further discussed, and the PN measurements for a generated RF carrier at 100 GHz are presented. The results confirm the low noise operation of the scheme approaching that of an ideal frequency multiplier, with an excess timing jitter with respect to a 20 GHz reference LO limited to only 2 fs. The electro-optical characterization of the assembled PIC-PCB sub-modules in a thermally-stabilized and fiber pigtailed compact packaged prototype is also provided.

Manuscript received...(Corresponding author: Claudio Porzi.)
This work is partially supported by the EU under the Italian National Recovery and Resilience Plan (NRRP) of NextGenerationEU, partnership on "Telecommunications of the Future" (PE00000001 – program "RESTART"), and by the Italian Ministry of Enterprises of Made In Italy through the ISOTTICA project.
Claudio Porzi is with TeCIP Institute, Scuola Superiore Sant'Anna, 56124 Pisa, Italy (e-mail: claudio.porzi@santannapisa.it).
Marco Chiesa, Aina Serrano Rodrigo, and Davide Rotta are with Camgraphic Srl, 56124 Pisa, Italy. (e-mail: aina.serrano.rodrigo@camgraphic-technology.com; marco.chiesa@camgraphic-technology.com).
Alessandra Bigongiari and Antonio D'Errico are with Ericsson Research, 56124 Pisa, Italy (e-mail: alessandra.bigongiari@ericsson.com; antonio.d.errico@ericsson.com).
Luca Roselli is with the Department of Engineering, University of Perugia,06125 Perugia, Italy (e-mail: luca.roselli@unipg.it).
M. Sorel is with the School of Engineering, University of Glasgow, Glasgow G12 8QQ, U.K., and also with the TeCIP Institute, Scuola Superiore Sant'Anna, 56124 Pisa, Italy (e-mail: marc.sorel@glasgow.ac.uk).
Antonella Bogoni is with TeCIP Institute, Scuola Superiore Sant'Anna, 56124 Pisa, Italy, and also with PNTLab, CNIT, 56124 Pisa, Italy (e-mail: antonella.bogoni@santannapisa.it).
Antonio Malacarne is with PNTLab, CNIT, 56124 Pisa, Italy (e-mail: antonio.malacarne@cnit.it).

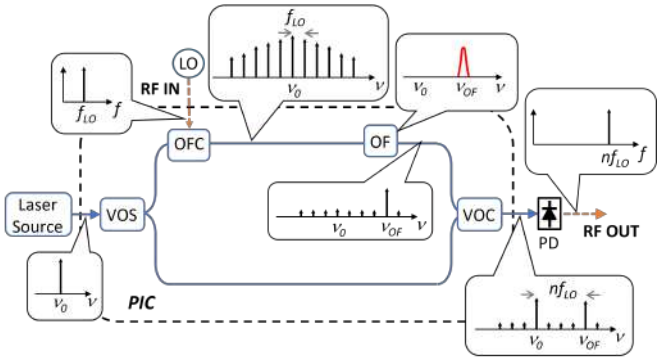

Fig. 1. Schematic operation of the photonic integrated RF synthesizer. PIC: photonic integrated circuit; VOS: variable optical splitter; OFC: optical frequency comb; OF: optical filter; VOC: variable optical coupler; PD: photodiode.

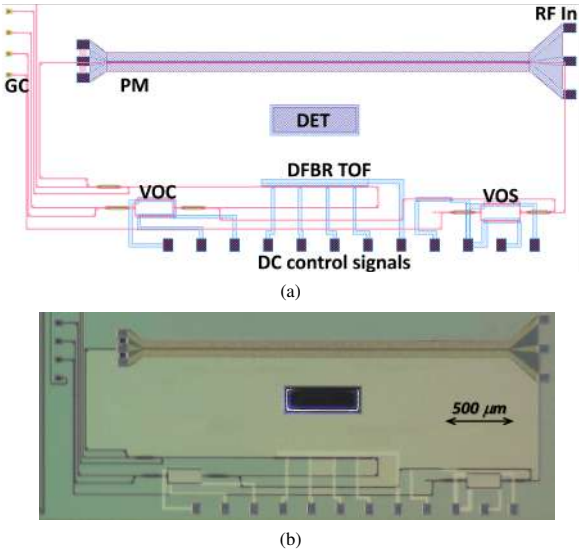

(a)

(b)

Fig. 2. (a) Mask layout of fabricated photonic integrated circuit in silicon-on-insulator technology. GC: grating coupler; PM: phase modulator; VOS: variable optical splitter; DFBR TOF: distributed feedback resonator tunable optical filter; VOC: variable optical coupler; DET: deep-etch trench. (b) Micrograph of fabricated sample.

II. PIC Design and Implementation

The operation of the photonic integrated RF synthesizer is illustrated in Fig. 1. In the scheme, part of the light injected into the PIC from an external laser source is delivered to an electro-optic OFC source driven by a LO signal with frequency f_{LO}, and followed by a bandpass tunable optical filter. The integrated optical filter then isolates a single harmonic out of the comb spectrum, which is subsequently recombined with the original carrier at the PIC output. Two optical tones frequency-spaced by an integer multiple n of f_{LO}, being n the order of the comb harmonic selected from the filter, are then obtained at the output of the PIC. Subsequent beating of the two spectral components in a high-speed PD generates the frequency-multiplied RF signal.

The mask layout for circuit realization through a multi-process wafer service in silicon-on-insulator technology using standard deep ultraviolet lithography [15] is shown in Fig. 2, along with a micrograph of the fabricated device. A 2 mm-long silicon photonics (SiP) phase modulator is employed for OFC generation, whereas the photonic integrated tunable filter is implemented through a compact multi-cavity distributed feedback resonator (DFBR) architecture based on coupled waveguide Bragg grating mirrors [16]. Grating couplers are used to access the input/output optical ports of the circuit as well as the monitor ports for components characterization through a fiber array.

Some slight, yet effective, variations with respect to our previous realization presented in [6], [14], are implemented in this new layout. At first place, the integrated optical splitter and coupler placed at the circuit input and output ports, respectively, are now made variable using thermally-controlled Mach-Zehnder interferometer structures. By acting on the input/output variable optical splitter and coupler, rather than using a variable optical attenuator on the carrier path as in [14], the impinging optical power can be efficiently routed through the circuit for careful control of the output optical carrier-to-selected-harmonic power ratio (CSHPR), while guaranteeing a fair optical power level of the filtered tone as the order of the selected OFC harmonic is varied. Controlling the CSHPR is advantageous for either maximizing the received RF power [17] or adjusting the overall circuit output power for minimized signal-spontaneous emission beat noise in the PD if optical amplification is used after the PIC [18]. In second place, always for the sake of maximizing the output optical power and PN performance, an optimized design of the waveguide filter aiming at simultaneously minimize the insertion loss, provide large suppression of spurious OFC harmonics, and increase the robustness against environmental fluctuations, is realized. To this scope, back-calibration of the relevant design parameters from measurements of previously realized DFBR samples is employed for synthesizing a bandpass response seeking the optimal trade-off between passband width, roll-off, and low insertion loss [5]. Additionally, for the ease of operation, the floorplan of the circuit has been arranged for minimizing the thermal interaction between its main building blocks, and an air-filled deep-etch trench through the full stack and down 60 μm into the silicon substrate is placed between the tunable filter and the phase modulator-based OFC, such to mitigate the filter wavelength drift as the modulator driving RF power and bias conditions are adjusted. The spatial extension of the deep-etch trench is limited in this realization by the design constraints for this specific fabrication process. Finally, in view of the assembling of the PIC with the electronic control board and the final packaging of the RF synthesizer, the position and spacing of the RF electrical pads is chosen to guarantee a low loss and low inductive-loading wire-bonding with the signal lines on the PCB.

III. Bare Chip Characterization

A. DFBR Photonic Integrated Filter and OFC Source Characterization

Preliminary on-chip testing of the circuit components through monitor input/output optical ports, and of the full-scheme RF operation is then performed. The measured trans-

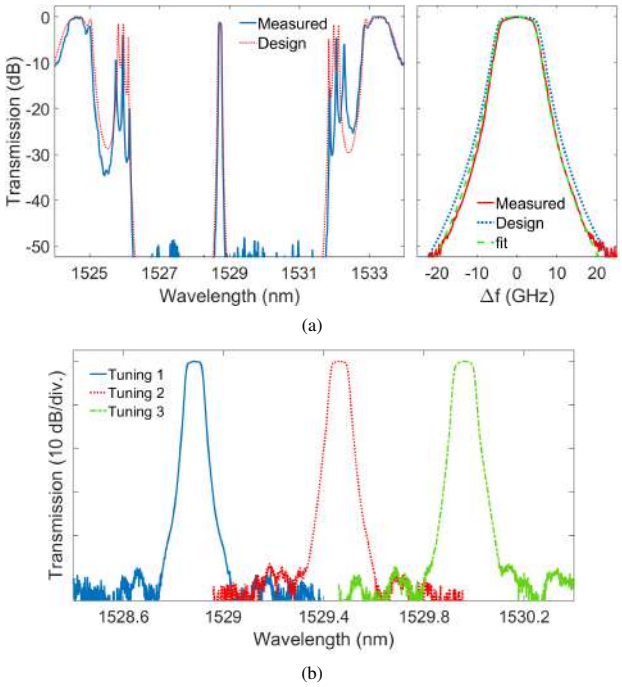

Fig. 3. (a) Wide-span spectral transmission of the distributed feedback resonator (DFBR) tunable optical filter (left) and detail of the normalized bandpass window around its central frequency versus normalized detuning Δf (right). (b) Tuning of the DFBR filter passband.

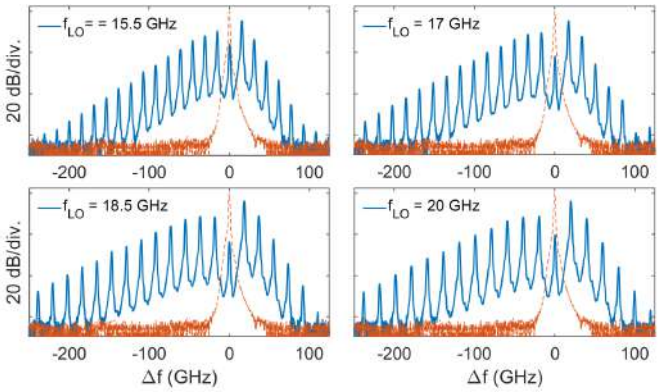

Fig. 4. Optical frequency comb (OFC) source output spectra with (solid lines) and without (dashed lines) applied RF power for different values of local oscillator (LO) driving frequency, f_{LO}, with ∼1W power delivered to the contact probes. The traces are reported versus frequency deviation Δf from the optical carrier and normalized to its peak power (non optimal probe contacting is observed for the 15.5 GHz trace).

mission spectrum of the DFBR optical filter over a wide wavelength span and the details of the passband window are shown in Fig. 3(a). The target design simulation is also shown in the figure, along with the numerical fit of the passband region. From the measurements, a wide −40 dB stopband of about 6.4 nm is observed, whereas the −3 dB passband width is 8.5 GHz, and the out-of-band rejection at 20 GHz from the central frequency is as large as 50 dB (roll off: ∼3.7 dB per GHz). Finally, a remarkably low insertion loss of ∼1.2 dB around the flat passband peak for this 4$^{\text{th}}$-order architecture is measured. These numbers confirm that high-performance photonics-based processing of RF signals over a wide instantaneous bandwidth of several hundreds of GHz can be achieved through DFBR filter technology, for which passband widths down to about 1 GHz have been demonstrated [19]. The structure has been targeted for optimized operation in combination with the OFC source, as discussed ahead, and the agreement between the measured and design traces confirms the maturity of the DFBR design process, also relying on the extrapolation of the main grating parameters from previously realized devices [14], [19], [20]. From the numerical fit of the passband window, a non-influential deviation from the target design for the fabricated grating coupling strength of less than 4% is calculated.

Continuous adjustment of the filter passband central wavelength within the stopband region is achieved by means of micro-heaters that individually control the optical path length of the coupled cavities between the distributed mirrors [14], [16]. An example of the photonc-integrated filter tuning is shown in Fig. 3(b), for a measured overall tuning efficiency of the four micro-heaters of 0.15 mW/GHz.

The other pivotal component for circuit operation is the SiP OFC source. A single phase modulator-based solution is employed for this element, due to the simplicity of the operation and minimized footprint with respect to more complex architectures and considering that having a flat comb response is not of primary interest for this application. Rather, the main role of the OFC source is to maximize the power of the intended harmonic to be selected. Considering the cut-off frequency of about 20 GHz for this 2 mm-long SiP modulator [14] operating in carrier-depletion mode, the system was designed to attain the W-band with a maximum multiplication factor of the input LO frequency of 6, permitting to manatain a relatively large level of the selected OFC tone spectral power. This is illustrated in Fig. 4, reporting the OFC output spectra for different values of f_{LO}, ranging from 15.5 to 20 GHz, and using an RF amplifier to boost the power level of the signal delivered to the probes contacting the modulator electrodes to about 30 dBm. A DC signal with typical voltage level of about 3.5 V for reverse biasing the pn-junction in the SiP modulator is also coupled to the LO signal through a bias-tee. The OFC spectra are normalized to the optical carrier peak power level at the output of the device in absence of the modulating signal, which is also displayed in the figures. For the 15.5 GHz curve, the poor depletion of the carrier might indicate a non perfect contact between the probe and the ground-signal-ground (GSG) pads connected to the modulator traveling line. Apart this discrepancy, the plots indicate that comb tones spaced between 75 and 110 GHz from the optical carrier (that is, the extremes of the W-band) can be obtained with a modulation efficiency (i.e., the ratio between the relevant harmonic and input carrier power) comprised between −20 and −25 dB, where the ∼2.5 dB insertion loss of the depleted modulator are also taken into account.

B. RF synthesis performance evaluation

The relevant metrics of the mm-wave band RF synthesizer are then evaluated using a representative value of 20 GHz for f_{LO} and a generated mm-wave band carrier of 100 GHz. The

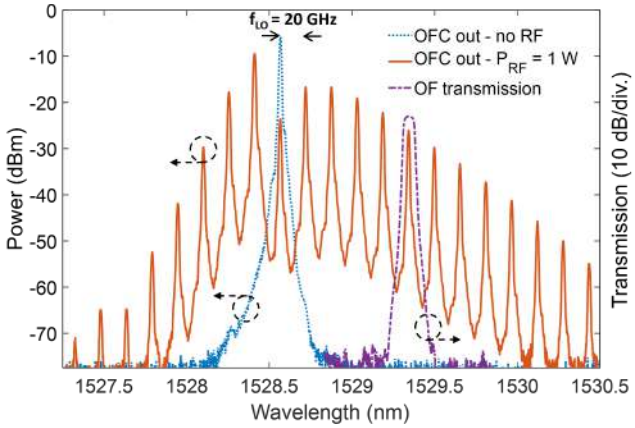

Fig. 5. Optical frequency comb (OFC) output spectrum with (solid line) and without (dotted line) applied local oscillator (LO) signal at $f_{LO} = 20$ GHz, and distributed feedback resonator (DFBR) filter transmission window (dash-dotted line) when tuned to select the longer-wavelength 5th-order comb harmonic.

corresponding OFC source output spectrum (with and without applied LO signal), along with the bandpass response of the DFBR filter tuned to select the 5th-order longer-wavelength harmonic from the comb, are shown in Fig. 5. The optical spectrum of the composite signal at the PIC output obtained by recombining the selected sideband with the original laser carrier for two different conditions of CSHPR is then shown in Fig. 6.

For the case of equalized tones (CSHPR: ~ 0 dB) of Fig. 6(a), a large minimum rejection level of 38.6 dB for the spurious harmonics is measured. For the situation depicted in Fig. 6(b), the measured carrier power (over 0.01 nm resolution bandwidth) is raised with respect to the previous case from -29 dBm to -20.5 dBm, whereas the filtered harmonic level is slightly reduced from -29.3 dBm to -31.7 dBm, so that the CSHPR is now 11.2 dB. The minimum spurious harmonic rejection is correspondingly reduced to 31.2 dB. At the same time, an overall larger optical power is now attained at the circuit output, without sacrificing too much the optical signal to noise ratio of the selected harmonic. For these measurements, the carrier power from the laser source at the PIC input, measured on the same resolution bandwidth of 0.01 nm, is ~ 10 dBm. The coupling loss of the input/output grating couplers pair is measured to be about 9 dB. An additional power loss source slightly larger than 3 dB is due to the presence of a 2×2 multimode interference directional coupler on the modulator path providing the monitor input/output ports for the integrated filter and OFC source.

The PN performance of the continuous-wave signal obtained by injecting the PIC output into a high-speed PD is then measured through a signal source analyzer using the set-up shown in Fig. 7. In order to overcome the nominal bandwidth of 7 GHz of the analizer (Agilent E5052A), a heterodyne detection technique employing a 26.5 GHz-bandwidth down-converter (Agilent 5053A), in conjunction with harmonic mixers (Keysight 11970W) is adopted, thus extending the measurement range up to about 110 GHz. Considering the large insertion loss of around 50 dB of the microwave downconverter,

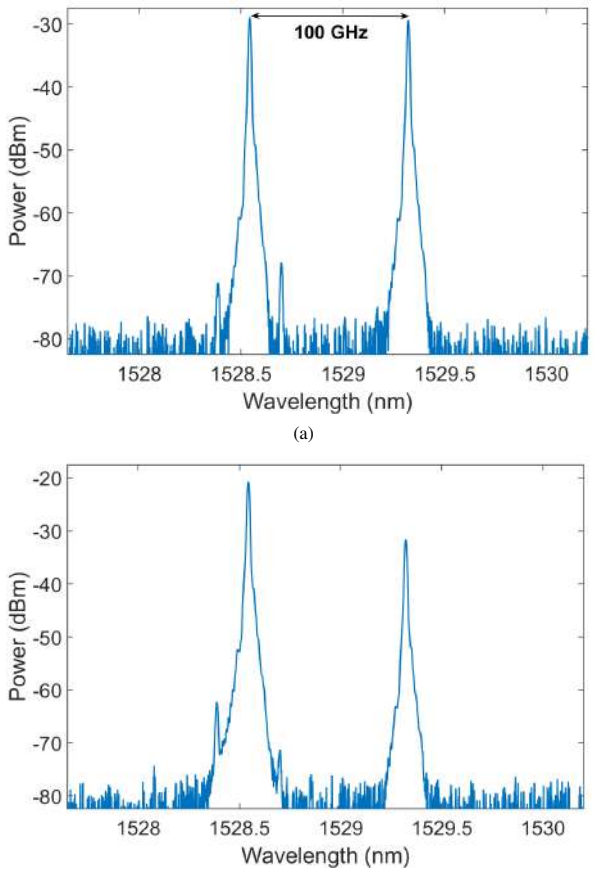

Fig. 6. Photonic integrated circuit (PIC) output spectra corresponding to the traces of Fig. 5 with filter tuned to select a comb harmonic spaced 100 GHz from the the optical carrier. Two different carrier-to-selected harmonic power ratio (CSHPR) of (a) ~ 0 dB and (b) ~ 10 dB are illustrated.

an erbium-doped fiber amplifier (EDFA, IPG Photonics EAD-10-C3) is used to rise the optical power at the input of the PD (u^2t XPDV4120R, with 90 GHz electrical 3 dB bandwidth) to about 6 dBm. An optical bandpass filter (an Optoquest cassette embedding a 1 nm-wide oxide dielectric-type filter) is also employed to band-limit the amplified spontaneous emission

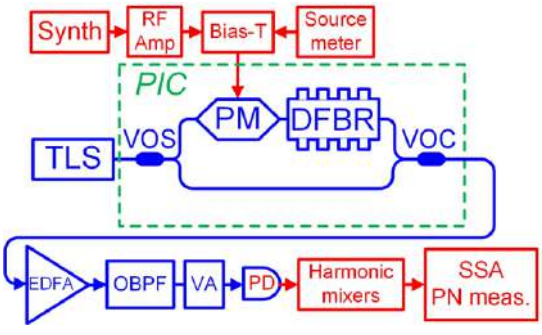

Fig. 7. Experimental set-up for the phase noise (PN) characterization of the photonic-integrated mm-wave band RF synthesizer. TLS: tunable laser source; VOS: variable optical splitter; PM: phase modulator; DFBR: distributed feedback resonator; VOC: variable optical coupler; EDFA: erbium-doped fiber amplifier; OBPF: optical bandpass filter; VA: variable attenuator; PD: photodiode; SSA: signal source analyzer; Synth.: synthesizer; Amp.: RF amplifier.

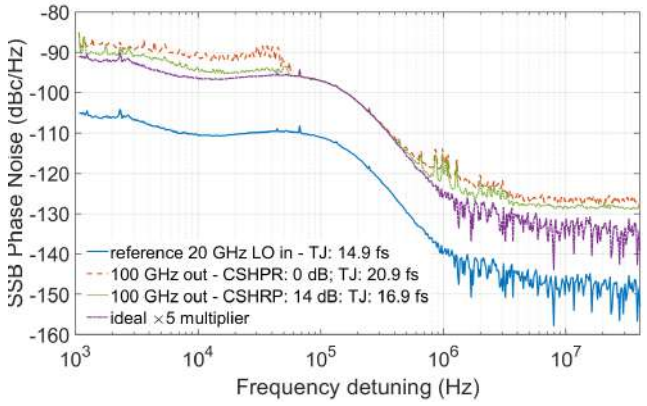

Fig. 8. Mesaured phase noise (PN) for the synthesized 100 GHz RF carrier under two different conditions of optical carrier-to-selected harmonic power ratio (CSHPR).The PN of the reference input local oscillator (LO) signal at 20 GHz and the theoretical curve of an ideal ×5 frequency multiplier are also reported. The corresponding timing jitter (TJ) values, calculated over the displayed frequency range, are also indicated for the different cases.

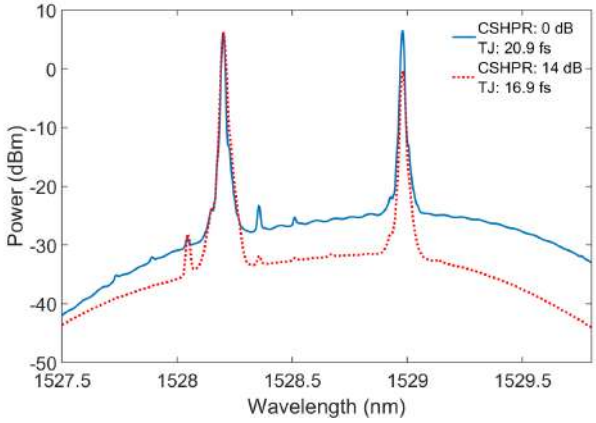

Fig. 9. Optical spectra of the beating tones at the photodiode input after optical amplification stage for the two values of carrier-to-selected harmonic power ratio (CSHPR) measured at the circuit output reported in the phase noise power spectral density curves of Fig. 8. The corresponding calculated timing jitter (TJ) values are also indicated.

(ASE) noise from the EDFA. During the measurements, the PIC temperature is stabilized using a Peltier cell controlled by a thermistor-based feedback loop.

The measured PN power spectral density in the range 1 kHz – 40 MHz of frequency offset from the carrier under test is then shown in Fig. 8, for two different values of the CSHPR at the PIC output. The PN characteristic of the 20 GHz LO and that of an ideal frequency multiplier, obtained by up-shifting the reference LO curve by $10\times log_{10}(m^2)$, being m the multiplication factor (5 in this case), are also reported.

The deviation in the measured PN of the synthesized signals with respect to the benchmark ideal frequency multiplier curve at low frequency detuning range (below $\sim$ 50 kHz) originates from small oscillations of the DFBR filter central frequency associated to residual temperature fluctuations that could not be completely tackled by the thermoelectric cooler system, and by the noise of the DC source meters employed for tuning the filter [6]. On the other hand, the PN floor on the high frequency side is bounded for the measured 100 GHz traces by the available optical signal-to-noise ratio which is primarily limited in our setup by the optical amplification stage. Both these terms then contribute to degrade the timing jitter (TJ) of the 100 GHz carrier with respect to that of the LO reference at 20 GHz, which is measured to be 14.9 fs through integration of the corresponding PN power spectral density over the considered 1 kHz – 40 MHz range. However, by adjusting the relative amplitude of the two impinging tones, both the low- and high-frequency noise contributions can be minimized, as shown in the figure. For the case of equalized beating tones at the input of the amplifier, the measured TJ is indeed $\sim$ 21 fs whereas, departing from this situation, an optimized power imbalance between the two components permits to reduce the TJ down to 16.86 fs.

This behaviour can be explained by observing the optical spectra of the signal delivered to the PD for the two cases, which are shown in Fig. 9. It can be seen that, when the optical carrier and selected harmonic are equalized, a larger level of ASE is present with respect to the case in which the lowest TJ is measured, corresponding to unbalanced beating tones. In this latter case, indeed, the optical power level of the carrier at the PIC output is ~ -17 dBm (at 0.01 nm resolution bandwidth), about 14 dB larger than the filtered comb harmonic, whereas the equalized tones share a power level at the PIC output bounded to about -30 dBm, as previously discussed. Therefore, the optical amplifier gets more saturated with the optimized CSHPR and the ASE level correspondingly decreases. This reduces both the measurement noise floor in the high frequency range as well as the contribution to the excess PN in the range 0 – 50 KHz originating from the beating terms in the output PD between the amplifier noise and the selected harmonic. Additionally, since the condition of equalized tones corresponds to maximizing the portion of light emerging from the modulator path at the PIC output (if we exclude the unfavorable cases of negative CSHPR values), a larger contribution of the beating between the noisy harmonic and residual carrier after filtering is obtained in this case. Although an equalized power level of the beating

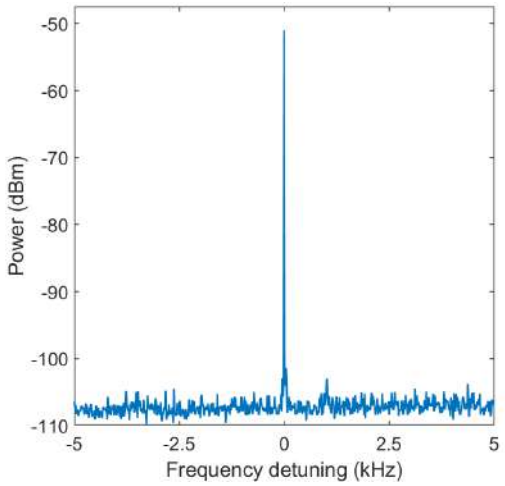

Fig. 10. Measured RF spectrum of the generated 100 GHz carrier.

tones in the PD would maximize the received RF power for a given level of detected optical power [17], the effect of optical amplification in a practical system should be also taken into account, and the proposed mm-wave band clock synthesizer confirms its flexibility in controlling the relevant system parameters for optimized PN performance. Finally, the 100 GHz RF spectrum obtained from the SSA using a resolution bandwidth of 25 KHz, and corresponding to the case of optimized PN performance, is reported in Fig.10, illustrating a signal-to-noise ratio of more than 50 dB.

Both the PN and the signal-to-noise ratio features of the generated RF carrier can be expected to further improve by raising the available optical power level at the PIC output for both the carrier and selected harmonic simultaneously. This would permit to drive the subsequent EDFA in deeper compression for minimizing the ASE-related beating terms and approach the shot-noise limit for the output RF noise level [18], while at the same time increasing the useful optical power available for RF generation at the PD input. To this scope, an advanced circuit version would benefit from low-loss edge or grating couplers to reduce the coupling losses [23], [24], tunable splitters for the filter and OFC source monitor ports to minimize path losses, and optimized SiP modulator waveguide doping profile for maximizing the comb generation efficiency [25].

It should be also noticed that, as evident from the spectral traces of Fig. 3, the the distributed mirrors in the current DFBR filter operate at around 1530 nm, where EDFAs typically exhibit a noisier characteristic and a lower gain with respect to the 1550 nm region, despite using the same corrugation period as in previous recent similar grating realizations leading to a Bragg wavelength of 1550 nm [14], [20], [22]. Such a large wavelength shift cannot be accounted for with the provided maximum deviations of the waveguide effective index from nominal value for this fabrication process and, although still under investigation, we ascribe it to possible wafer-to-wafer variations in the thickness of the silicon layer. Even though the absolute value of the DFBR central wavelength does not affect the operation principle of the circuit, further improvement of its PN performance in presence of EDFA-based optical amplification can be expected for a system operating at around 1550 nm.

IV. Electro-Optic Packaging of the mm-wave band RF Synthesizer

A. PCB design and assembly with PIC

The electro-optic package of the PIC-based mm-wave band clock synthesizer involved at first the development of a PCB carrying the relevant RF and DC signals driving and controlling the various on-chip OFC source, tunable optical filter, and variable optical coupler and splitter. In particular, the LO signal at microwave frequencies and the DC reverse bias of the p-n junction in the SiP modulator waveguide are delivered to the PIC through an integrated on-board bias-tee. A custom design is developed to support the large power dissipation levels at the termination load of the modulator traveling-wave line of up to about 2 W associated to the RF and DC bias

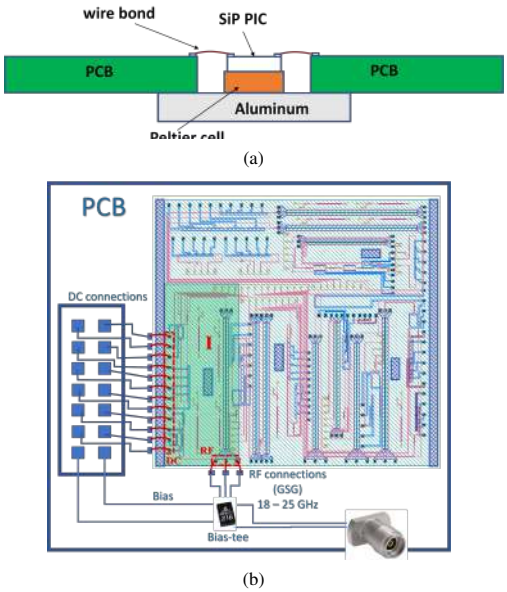

Fig. 11. Schematic (a) cross-section and (b) top-view design concept for the developed printed circuit board (PCB) – silicon photonics (SiP) photonic integrated circuit (PIC) assembly.

signals. Additionally, a broadband matching condition of more than 6 GHz is pursued for improving the flexibility of the RF synthesizer by permitting an optimized choice of the reference LO frequency and of the frequency multiplication factor for a given target mm-wave output signal. A broadband design would also enable the operation in presence of high-speed modulated RF data signals driving the electro-optic modulator [14].

The cross-section and top-view of the designed packaging concept, including an aluminum protective box providing also the required physical support for the different components of the assembly is shown in Fig. 11. On the PIC side, the GSG pads connecting the p- and n-doped contacts of the modulator through the transmission line are placed at the chip edge with a pitch of 200 μm. The corresponding RF pads on the PCB have a slightly lager pitch due to design constraints,

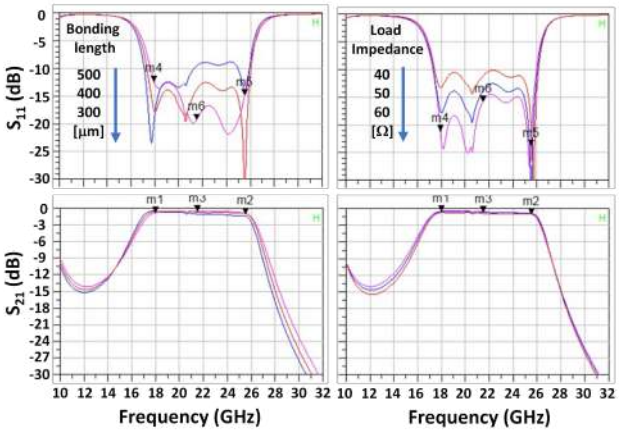

Fig. 12. Simulation results for the *S*-parameters of designed bias-tee matching network.

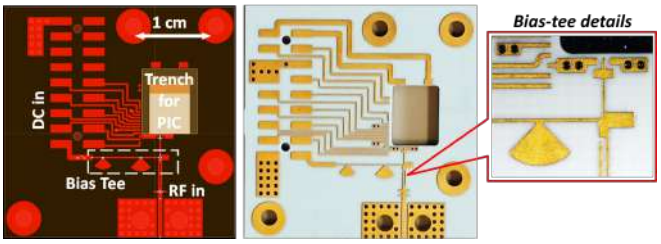

Fig. 13. Designed (left) and fabricated (right) printed circuit board (PCB).

and are connected through a coplanar waveguide to the RF input port of the board where contact pads are realized for mounting a K-type connector to input the LO signal. The relevant transition between the circuit microstrip and coplanar lines has been optimized too. The array of DC pads on the PIC side is placed perpendicular to the modulator GSG pads, and the corresponding lines on the PCB carrier terminate to a pad array matching the pins of a Molex connector. The stack layers in the board are chosen such that the PCB and PIC surfaces are on the same plane, also considering the underlying Peltier cell for thermo-electric stabilization of the module. This ensures that both ends of the wire bonds are in the same plane, which helps in minimizing the parasitic inductive impedance unavoidably introduced by wire bonding and in guaranteeing the repeatability of the wire length. A rectangular trench is created inside the board to host the PIC, so as to minimize the gap between the two chips therefore enabling a nominal wire length from PIC to carrier of about 300 μm.

For the design of the matching network, we departed from the measured frequency response of the input impedance of the coplanar waveguide in the SiP modulator, that is terminated on a voltage-dependent doped silicon resistance, with typical operating bias conditions between 3 and 4 V. To guarantee the signal integrity along the interconnection, the effects of wire-bonds between the RF pads on the PCB and PIC are also included accordingly to the model presented in [21].

The designed *S*-parameters of the bias-tee interconnection network obtained from a finite-element full-wave simulation are reported in Fig. 12. The variations around nominal values of the wire-bond length as well as of the input impedance of the transmission line carrying the driving signal in the SiP phase modulator are also considered. From the S_{11} parameter, a maximum return loss below about 10 dB between 18 GHz and

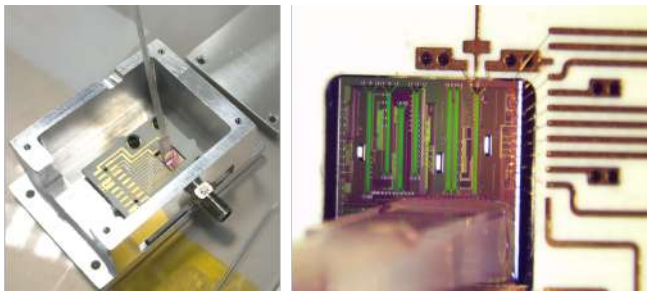

Fig. 14. Packaged photonic integrated-based mm-wave band RF synthesizer prototype.

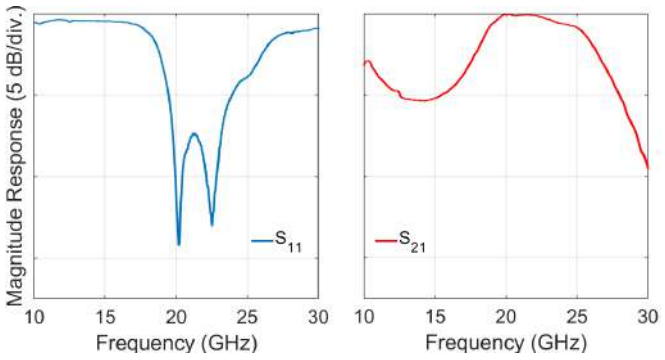

Fig. 15. Measured *S*-parameters of the packaged printed circuit board (PCB) – photonic integrated circuit (PIC) system.

26 GHz can be expected for this first-guess simulation under the various conditions, corresponding to a drop of about 3 dB at the edges of this range in the S_{21} parameter curve.

The designed PCB layout and a picture of the fabricated sample along with the details of the bias-tee section are then shown in Fig. 13. The RF and DC pads on the photonic chip die and PCB have then been connected through wire bonds to realize electrical connections. Finally, access to the input/ouput optical signals is provided by pigtailing a fiber array to the on-chip grating couplers using an automatic active alignment bench. A picture of the packaged prototype is shown in Fig. 14, where a close-up view of the wire bonds and attached fiber array are also visible.

B. Characterization of the Packaged Device

Signal integrity for the packaged sample has been at first verified by measuring the *S* parameters of the electro-optic assembly using a two-ports vector network analyzer connected to the RF input of the device and to an external photodiode collecting the light at the PIC output. In order to convert the output of the on-chip phase modulator to useful amplitude-modulated signal, the input laser wavelength is adjusted for bypassing the photonic-integrated filter, so that the scheme operates as a single arm-driven Mach-Zehnder interferometer

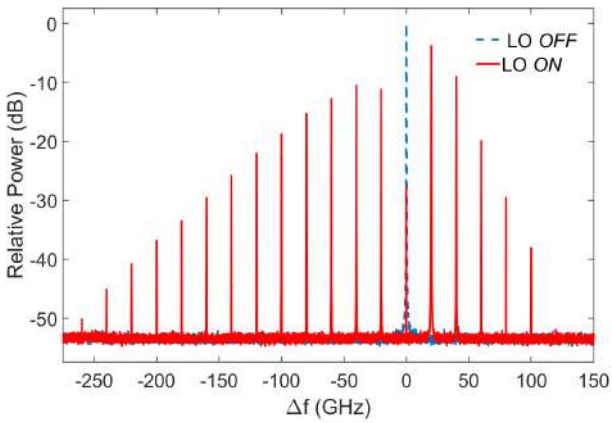

Fig. 16. Output spectrum of the packaged on-chip optical frequency comb generator with and without applied local oscillator (LO) signal versus frequency detuning Δf from input optical carrier.

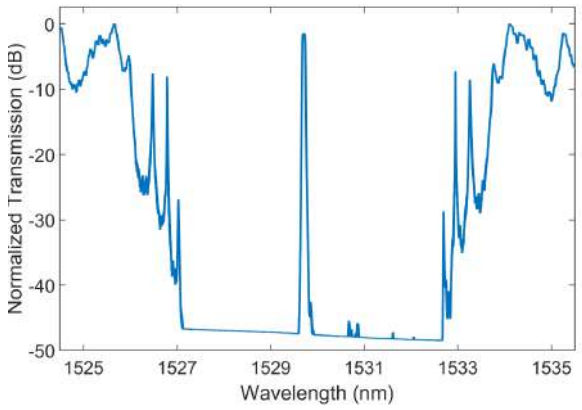

Fig. 17. Measured transmission spectrum of the packaged on-chip photonic-integrated filter.

[22]. The results of the measurements are reported in Fig. 15. The S_{11} parameter exhibits a slight up-shift of the target central frequency of the matching network and a somewhat higher return loss and shrinking of the operating bandwidth with respect to the simulation results. This is ascribed to the observed over-etch of the fabricated RF lines in the PCB that, as observed from the details of the sample reported in Fig. 13, caused a deviation for the bias-tee capacitor from the ideal fill factor of 50%. The S_{21} curve, including the electro-optic and opto-electronic RF conversion loss, shows a flat maximum response at frequencies between $\sim$20 and 22.5 GHz, and is reduced by 1 dB at 25 GHz, above which the RF insertion loss further increase due to the combined action of unmatched condition and modulator roll-off. Nevertheless, the operation using a LO tone at 20 GHz is preserved, as confirmed by the measured comb spectra of the packaged OFC source reported in Fig.16, where the curves are again normalized to the unmodulated signal level at circuit output. A fair power conversion efficiency of the input optical carrier level (taking into account modulator insertion loss) of around 20 dB at 100 GHz can be observed, using an RF power level of $\sim$1.5 W, which is slightly larger than what required for the the bare chip at the same efficiency level. Based on the measured width of the fabricated RF traces, a calibrated design for the fabrication process under consideration has been produced and used for realizing a second PCB version with expected improved performance that is currently in progress. Finally, the results of the packaged photonic integrated filter characterization are reported in Fig. 17.

V. Conclusion

A packaged millimetre-wave band RF synthesizer based on a photonic integrated circuit in silicon-on-insulator technology is realized and experimentally verified. Operation in the W-band is specifically targeted for this realization. The device accepts at its input a laser and a microwave carrier to provide at its output a spectrally-pure signal comprising two optical tones with large signal-to-noise ratio that are separated by an integer multiple of the reference local oscillator. This signal is thus suitable for being transmitted toward a remote photodiode for efficient and low-loss distribution of high-quality RF clocks in fiber links and networks, without suffering from RF power fading effect. The package comprises a printed circuit board which is wire-bonded to the photonic chip and encompasses a custom-developed bias-tee designed to support large power levels and to operate over several GHz for the local oscillator signal. Fiber pigtails, RF connectors, and thermo-electric cooling are also included in the assembly. Besides compactness and flexibility in the RF synthesis operation, a low phase-noise characteristic for the generated signal is one of the main features of the proposed circuit, which makes it suitable for high-data-rate wireless transmissions and high-resolution sensing and imaging applications. At 10 kHz offset from a generated 100 GHz carrier wave a phase noise level of -97 dBc/Hz is measured, matching the value that is obtained by an ideal frequency multiplication of a local oscillator signal at 20 GHz. Other noise contribution at larger and lower frequencies offset can be minimized under different conditions of subsequent optical amplification thanks to the possibility of carefully controlling the characteristics of the circuit output signal.

References

[1] J. Hulme et al. "Fully integrated microwave frequency synthesizer on heterogeneous silicon-III/V." *Opt. Express*, vol. 25, no. 3, pp. 2422-2431, Feb. 2017.

[2] M Rahim et al., "Monolithic InAs/InP quantum dash dual-wavelength DFB laser with ultra-low noise common cavity modes for millimeter-wave applications," *Opt. Express*, vol. 27, no. 24, pp. 35368-35375, Nov. 2019.

[3] Y. Liu, Q. Tang, L. Zhang, X. La, L. Zhao, W. Wang, and S. Liang, "Dual-wavelength DBR laser integrated with high-speed EAM for THz communications," *Opt. Express*, vol. 28, no. 7, pp. 10542-10551, Mar. 2020.

[4] R. Guzmán et al. "Widely tunable RF signal generation using an InP/Si_3N_4 hybrid integrated dual-wavelength optical heterodyne source," *J. of Lightw. Technol.*, vol. 39, no. 24, pp. 7664-7671, Dec. 2021.

[5] C. Porzi, F. Falconi, M. Sorel, P. Ghelfi and A. Bogoni, "Flexible millimeter-wave carrier generation up to the sub-THz with Silicon photonics filters," *J. of Lightw. Technol.*, vol. 39, no. 24, pp. 7689-7697, Dec. 2021.

[6] A. Malacarne, A. Bigongiari, A. D'Errico, A. Bogoni and C. Porzi, "Reconfigurable low phase noise RF carrier generation up to W-band in silicon photonics technology," *J. Lightw. Technol.*, vol. 40, no. 20, pp. 6891-6900, Oct. 2022.

[7] X. Zhu et al., "A novel high speed directly modulated dual wavelength 1.3 μm DFB laser for THz communications." *IEEE J. Sel. Topics Quantum Electron.*, vol. 29, no. 5, pp. 1-6, Sept.-Oct. 2023.

[8] A. Hallal, S. Bouhier, and F. Bondu. "Synthesis of a 30-Hz linewidth wave tunable over 500 GHz," *IEEE Trans. Microw. Theory Tech.*, vol. 65, no. 4, pp. 1367-1371, Apr. 2017.

[9] Fortier, T. M., et al. "Optically referenced broadband electronic synthesizer with 15 digits of resolution", *Laser Photonics Rev.*, vol. 10, no. 5, pp. 780-790, Sept. 2016.

[10] A. Ly, V. Auroux, R. Khayatzadeh, N. Gutierrez, A. Fernandez and O. Llopis, "Highly spectrally pure 90-GHz signal synthesis using a coupled optoelectronic oscillator," *IEEE Photon. Technol. Lett.*, vol. 30, no. 14, pp. 1313-1316, Jul. 2018.

[11] K. Sengupta, T. Nagatsuma, and D.M. Mittleman, "Terahertz integrated electronic and hybrid electronic–photonic systems", *Nat. Electron.*, vol. 1, pp. 622–635, Dec. 2018.

[12] A. Hirata, M. Harada and T. Nagatsuma, "120-GHz wireless link using photonic techniques for generation, modulation, and emission of millimeter-wave signals," *J. Lightw. Technol.*, vol. 21, no. 10., pp. 2145-2153, Oct. 2003.

[13] A. Malacarne et al., "Electro-optic packaging of silicon photonics-based RF multiplier for clock signal generation in the millimeter-wave band", *in Proc. 24th Eur. Conf. Integr. Opt. (ECIO)*, Enschede, The Netherlands, paper M2G, Apr. 2023.

[14] C. Porzi, F. Falconi, M. Sorel and A. Bogoni, "Broadband and high-capacity silicon photonics single-sideband modulator", *J. Lightw. Technol.*, vol. 40, no. 2, pp. 538-546, Jan. 2022.
[15] https://europractice-ic.com/mpw-prototyping/siphotonics/imec/
[16] C. Porzi, G. J. Sharp, M. Sorel and A. Bogoni, "Silicon Photonics High-Order Distributed Feedback Resonators Filters," *IEEE J. Quantum Electron.*, vol. 56, no. 1, pp. 1-9, Feb. 2020.
[17] B. Hraimel et al., "Optical single-sideband modulation with tunable optical carrier to sideband ratio in radio over fiber systems," *J. Lightw. Technol.*, vol. 29, no. 5, pp. 775-781, Mar. 2011.
[18] V. J. Urick, F. Bucholtz and K. J. Williams, "Noise penalty of highly saturated erbium-doped fiber amplifiers in analog links," textitIEEE Photon. Technol. Lett., vol. 18, no. 6, pp. 749-751, Mar. 2006.
[19] C. Porzi, M. Reza, M. Sorel and A. Bogoni, "Frequency and bandwidth tunable integrated microwave photonic bandpass filter," *2022 International Workshop on Fiber Optics in Access Networks (FOAN)*, Valencia, Spain, pp. 1-5, Oct. 2022.
[20] F. Falconi, C. Porzi, A. Malacarne, F. Scotti, P. Ghelfi and A. Bogoni, "UWB fastly–tunable 0.5–50 GHz RF transmitter based on integrated photonics," *J. Lightw. Technol.*, vol. 40, no. 6, pp. 1726-1734, Mar. 2022.
[21] F. Alimenti, P. Mezzanotte, L. Roselli, and R. Sorrentino, "Modeling and characterization of the bonding-wire interconnection," *IEEE Trans. Microw. Theory Tech.*, vol. 49, no. 1, pp. 142–150, Jan. 2001.
[22] C. Porzi, M. Reza, P. Ghelfi, M. Sorel and A. Bogoni, "Silicon-on-Insulator Microwave Photonic Filter With Widely Tunable and Reconfigurable Flat-Top Bandpass Functionality," *J. Lightw. Technol.*, vol. 40, no. 20, pp. 6666-6675, Oct. 2022.
[23] R. Takei, M. Suzuki, E. Omoda, S. Manako, T. Kamei, M. Mori, Y. Sakakibara, "Silicon knife-edge taper waveguide for ultralow-loss spot-size converter fabricated by photolithography," *Appl. Phys. Lett.*, vol. 102, no. 10, Art. no. 101108, Mar. 2013.
[24] D. Benedikovic, et al., "High-directionality fiber-chip grating coupler with interleaved trenches and subwavelength index-matching structure," *Opt. Lett.*, vol. 40, no. 18, pp. 4190-4193, Sept. 2015.
[25] J. Sun, R. Kumar, M. Sakib, J. B. Driscoll, H. Jayatilleka and H. Rong, "A 128 Gb/s PAM4 Silicon Microring Modulator With Integrated Thermo-Optic Resonance Tuning," *J. Lightw. Technol.*, vol. 37, no. 1, pp. 110-115, Jan. 2019.

Claudio Porzi Claudio Porzi received the Laurea degree in electronics engineering from the "La Sapienza" University of Rome, Rome, Italy, in 2000, and the Ph.D. degree in telecommunications from Scuola Superiore Sant'Anna (SSSA), Pisa, Italy, in 2005. He is currently an Assistant Professor with SSSA, working on the design and characterization of photonic integrated circuits for microwave photonics and telecom/datacom applications. He has coauthored more than 150 research articles published in peer-reviewed journals or presented at major international conferences.

Marco Chiesa Marco Chiesa received the Laurea degree in nuclear engineering from Politecnico di Milano, Milan, Italy, in 2001 and the Ph.D. degree from the Department of Physics, University of Cambridge, Cambridge, U.K., in 2007. Between 2008 and 2014, he was a Postdoctoral Researcher with the Institutes of Micro Electronics and Material Science, Spanish National Research Council, Madrid, Spain. Since 2015, he has been with CamGraPhIC, formerly INPHOTEC Center, Scuola Superiore Sant'Anna, Pisa, Italy, where he develops and engineers processes for the assembly and packaging of electronic and photonic devices.

Alessandra Bigongiari Alessandra Bigongiari joined Ericsson in 2017. She is a senior researcher with a background in material science whose work at Ericsson primarily focuses on integrated photonics and optical technology. Bigongiari is the author of more than 20 filed patent applications and more than 30 publications in scientific journals. She holds a PhD in Physics from Ecole Polytechnique in Paris, France.

Aina Serrano Rodrigo Aina Serrano Rodrigo achieved her Engineer degree in Material science in 2014 and the Master degree in Mechanical Engineering in 2017, both at Universitat Politècnica de València (UPV, Spain). Since 2015, she has been working in the Assembly and Packaging Laboratories of the following organizations: Valencia Nanophotonics Technology Center, Fondazione INPHOTEC della Scuola Superiore Sant'Anna and currently at CamGraPhIC S.r.l. She has strong experience in the development of packaging technologies of photonics devices for terrestrial and space applications as well as in mechanical packaging design.

Marc Sorel Marc Sorel (Senior Member, IEEE) received the Laurea degree (cum laude) in electrical and electronics engineering and the Ph.D. degree in electronics and computer science from the Universitä di Pavia, Pavia, Italy, in 1995 and 1999, respectively. He joined the Optoelectronics Research Group with the University of Glasgow, Glasgow, U.K., in 1998. He was appointed a Professor of Optoelectronics in 2015. He was involved with the field of integrated photonic devices for more than 20 years. He has authored or coauthored more than 200 articles in peer-reviewed journals and he has made numerous presentations at major national and international conferences. He was with the scientific committees of several international conferences. His research interests include silicon photonics, semiconductor lasers, photonic integration, and mid-IR optoelectronic devices for sensing.

Davide Rotta Davide Rotta received the Laurea degree in Physics in 2011 and the PhD in Nanotechnology and Nanostructures in 2015 at University of Milano Bicocca. Then, he joined the INPHOTEC technology center in Pisa, where he developed a strong expertise in thin film manufacturing and advanced packaging of electronic and photonic integrated circuits for a wide range of applications, including datacom and telecom, sensors and space photonics. Since 2021, he is Clean Room Manager and Head of Advanced Packaging at CamGraPhIC Srl.

Luca Roselli Luca Roselli (Fellow, IEEE) joined the University of Perugia, Perugia, Italy, in 1991. In 2000, he founded the spin-off WiS Srl. He is currently a qualified Full Professor with the University of Perugia, where he teaches applied electronics and coordinates the High Frequency Electronics Laboratory. He has authored over 280 papers and Green RFID System (Cambridge University Press, 2014). His current research interests include HF electronic systems with special attention to RFID, new materials, and wireless power transfer. He is a member of the list of experts of the Italian Ministry of Research, the past Chair of the IEEE Technical Committees MTT-24-RFID, the Vice Chair of 25-RF Nanotechnologies, 26-Wireless Power Transfer, the ERC Panel PE7, the Advisory Committee of the IEEE-WPTC, and the Chairperson of the SC-32 of IMS. He is the Co-Chair of the IEEE Wireless Sensor Network Conference. He organized the VII Computational Electromagnetic Time Domain, in 2007, and the first IEEE Wireless Power Transfer Conference, in 2013. He is an Associate Editor of IEEE Microwave Magazine.

Antonio D'Errico Antonio D'Errico received the Ph.D. degree (cum laude) in telecommunication engineering from Scuola Superiore Sant'Anna, Pisa, Italy, in 2008. Since 2009, he has been with Ericsson Research as a Senior Researcher and currently a Specialist in photonics and telecommunication systems and also working on photonic-enabling technologies for 6G mobile networks. He is the author of more than 100 papers published in international journals, conference digests, and patents. His research interests include advanced technological solutions for optical networks. He is a Senior Member of OPTICA. He is on the board of reviewers for several international journals in optics and photonics.

Antonella Bogoni Antonella Bogoni is currently a Full Professor with Sant'Anna School-Italy, which is one of the pioneers of the Integrated Research Center for Photonic Networks and Technologies created in Pisa in 2001 by the School and CNIT (National Inter-University Consortium for Telecommunications). She is currently the Director of the CNIT National Laboratory on Photonic Networks and Technologies-PNTLab. From 2020 to 2021, she was technical responsible of the Integrated Photonic Technologies Center-INPHOTEC, a technology center for the fabrication and packaging of integrated photonic circuits and leader of the digital & microwave photonics area. She is author or co-author of 55 patents, two books, nine chapters and more than 200 papers on the main scientific international journals. She dedicated her research activity to photonics technologies for optical communication and sensing, with special focus on Security, Space, Automotive and precise agriculture applications. She got more than 50 national and international project grants with funding exceeding 13M€ and nine Best Paper awards. She is the Deputy Editor of Optics Letters and has been the General Chairman of the main international conferences of the sector.

Antonio Malacarne Antonio Malacarne received the M.S. degree (with Hons.) in telecommunication engineering from the University of Pisa, Italy, in 2004, and the Ph.D. degree (with Hons.) in emerging digital technologies from the Sant'Anna School of Advanced Studies, Pisa, Italy, in 2009. He was an Assistant Professor with the Sant'Anna School of Advanced Studies till 2020. He is currently Head of Research with CNIT – National Inter-University Consortium for Telecommunications, at the Photonic Networks and Technologies National Laboratory, Pisa, Italy, within the Microwave Photonics for Communication and Sensing area. He is a coauthor of more than 50 papers on international scientific journals, more than 160 papers on international conference proceedings, 12 international patents, and three book chapters. His scientific interests include optical signal processing of ultra-fast signals and optical transmission, and microwave photonics for remote sensing and biophotonics.